

Research Reports

Use and validation of epithelial recognition and fields of view algorithms on virtual slides to guide TMA construction

Sanford H. Barsky^{1,2}, Lynda Gentchev³, Amitabha S. Basu⁴, Rafael E. Jimenez³, Kamel Boussaid⁴, and Abhi S. Gholap⁴

¹Department of Pathology, University of Nevada School of Medicine, Reno, NV, USA, ²Nevada Cancer Institute, Las Vegas, NV, USA, ³Ohio State University College of Medicine, Columbus, OH, USA, and ⁴BioImage, Inc., Cupertino, CA, USA

BioTechniques 47:927-938 (November 2009) doi 10.2144/000113207

Keywords: epithelial recognition algorithms; fields of view; tissue microarrays; virtual slides; automation of construction

Supplementary material for this article is available at www.BioTechniques.com/article/113207.

While tissue microarrays (TMAs) are a form of high-throughput screening, they presently still require manual construction and interpretation. Because of predicted increasing demand for TMAs, we investigated whether their construction could be automated. We created both epithelial recognition algorithms (ERAs) and field of view (FOV) algorithms that could analyze virtual slides and select the areas of highest cancer cell density in the tissue block for coring (algorithmic TMA) and compared these to the cores manually selected (manual TMA) from the same tissue blocks. We also constructed TMAs with TMAker, a robot guided by these algorithms (robotic TMA). We compared each of these TMAs to each other. Our imaging algorithms produced a grid of hundreds of FOVs, identified cancer cells in a stroma background and calculated the epithelial percentage (cancer cell density) in each FOV. Those with the highest percentages guided core selection and TMA construction. Algorithmic TMA and robotic TMA were overall ~50% greater in cancer cell density compared with Manual TMA. These observations held for breast, colon, and lung cancer TMAs. Our digital image algorithms were effective in automating TMA construction.

Introduction

The high-throughput screening (HTS) revolution has taken center stage in cancer research: cDNA and oligo-spotted microarrays, proteomic blots, and tissue microarrays (TMAs) have become standard research tools (1–3). Of these three methodologies, TMAs represent an anachronism since both their construction and interpretation are manual and subjective rather than automated and truly high-throughput (4). Paradoxically, the need for reliable and efficient TMA creation and interpretation has increased for scientists discovering and validating putative cancer biomarkers (5). The final and ultimate proof of any putative cancer biomarker discovered by genomic or proteomic approaches lies in an evaluation of its pattern of in situ expression that only TMAs can provide. With the advent of digital pathology approaches and imaging technology that can scan whole microscopic slides into

virtual images with high resolution (6), we wondered whether mathematical insights into the morphology of cancer cell images in virtual slides might translate into imaging algorithms that could effectively guide the selection of the optimal areas of tissue for coring and the construction of TMAs. Because of the increasing demand for TMAs predicted to occur over the next decade and their expanding role in both biomarker discovery validation in cancer research (7)—and because one key rate-limiting step in the use of TMAs for this purpose is the time and effort it takes for their manual construction—we felt it would be highly desirable to automate their construction. Because we wanted to automate the construction of TMAs, we needed to create algorithms that could select cores with the highest proportion of epithelial cells (i.e., cancer cells) and that these algorithms needed to be at least as good as the manual selection of cores. After these algorithms were devised and evaluated, we were also able to construct

a robot to automate the construction of TMAs under algorithmic guidance.

Materials and methods

This study was reviewed by The Ohio State University College of Medicine Institutional Review Board (IRB) and approved (2006C0042).

Selection of cases

In this study, we retrieved 300 cases (consisting of two whole slides each and two corresponding paraffin blocks) of human breast cancer (100 cases), colon cancer (100 cases), and lung cancer (100 cases), which were used to make the different TMAs. Prior to TMA construction, each whole slide was scanned and made into a “virtual slide” and analyzed algorithmically. The algorithmic analysis consisted of applying a virtual “grid” to the image and dividing the slide into fields of view (FOVs) and subsequently analyzing each FOV with

epithelial recognition algorithms (ERAs) designed to quantitate the epithelial cell (cancer cell) percentages.

Image acquisition

Image acquisition utilized a scanner, either the Aperio ScanScope T2 System (Aperio, Vista, CA, USA) or the iSCAN System (BioImagene, Inc., Cupertino, CA, USA), which was capable of producing images with a resolution of 20 pixels/10 μm. Following image acquisition, images were screened for quality, enhanced and processed. For image acquisition, any commercially or freely available imaging system utilizing either a scanner or a microscope with attached digital or analog camera can be used, as long as the images are produced with a resolution of 20 pixels/10 μm.

Software for image analysis

For our overall approach of writing the software for image processing and analysis, we used Visual C++. With this software language we also created novel ERAs and FOV algorithms that recognize cancer cells and identify the areas of the slide with the highest density of cancer cells. The steps of the FOV and ERA algorithms (Supplementary Tables S1 and S2), as well as more-detailed flowcharts and descriptions of the algorithms (Supplementary Tables S3–S7) are provided.

Gridding of the virtual slide by the FOV algorithm

Each virtual slide was divided into a grid of squares (termed FOVs), each measuring 1 mm × 1 mm or 2000 pixels × 2000 pixels (Figure 1). The tissue slices appearing on glass slides exhibited a wide range of sizes but each could invariably be overlaid by a grid. The FOVs within the grid were individually analyzed (Supplementary Table S1). This approach ensured that the dimensions of each FOV were less than or equal to the predefined dimensions for FOV (2000 × 2000 pixels). On a given slide there could be several pieces of tissue each termed an area of interest or identification (AOI). In that case, each AOI was gridded and divided into FOVs of equal dimensions. Some AOIs, upon gridding, contained FOVs with little or no tissue, since the grid overlay was a collection of squares and the tissue fragment border usually irregular. At a designated threshold for the ratio of tissue to no tissue in a given FOV, that FOV could be blocked from further analysis. Alternatively, separate AOIs could be virtually merged before

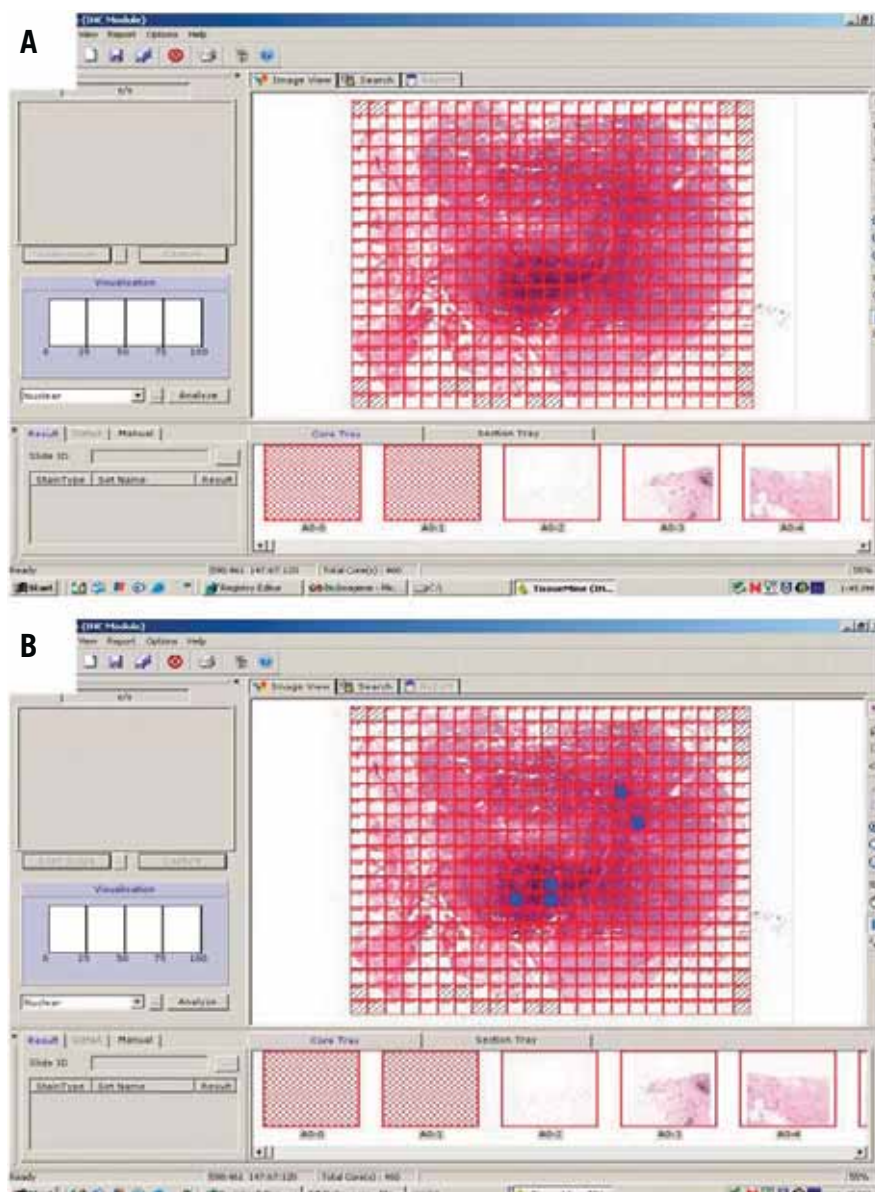


Figure 1. Algorithmic FOV and ERA analysis of a virtual slide guides TMA construction. Gridding of a virtual slide by the FOV algorithm is depicted (A). Each square area, termed FOV, is 1 mm² (2000 × 2000 pixels) and approximates the size of a TMA core. The FOV can be individually analyzed and compared with each other. Epithelial percentage (cancer cell density) is calculated and the FOV are ranked. The five FOVs ranked highest are marked in blue (B) and areas corresponding to these FOVs on the paraffin blocks are either manually cored (algorithmic TMA) or cored by TMAker (robotic TMA).

Table 1. Intra-class correlations for epithelial percentages on FOVs on whole slides across various tissues

Tissue	Number of cases	Raters	Intra-class correlation (95% confidence interval)
Breast	100	Algorithm vs. A ^a	0.86 (0.77, 0.95)
		Algorithm vs. B ^b	0.92 (0.86, 0.98)
		A vs. B	0.90 (0.88, 0.92)
Colon	100	Algorithm vs. A	0.85 (0.77, 0.93)
		Algorithm vs. B	0.89 (0.79, 0.99)
		A vs. B	0.92 (0.87, 0.97)
Lung	100	Algorithm vs. A	0.84 (0.82, 0.86)
		Algorithm vs. B	0.86 (0.81, 0.91)
		A vs. B	0.89 (0.87, 0.91)

^aA represents an individual rater (first pathologist); ^bB represents another rater (second pathologist).

gridding was performed; where appropriate, blocked FOVs could then be unblocked if the merged image produced a greater ratio of tissue to no tissue.

Quality of image evaluation

Each grid was first analyzed for image quality. Not every acquired image was of sufficient quality to be further evaluated. There were several criteria that determined image quality: luminosity, sharpness, and contrast. A number of techniques could be used to improve image quality and normalize image variations (8–10). With these techniques, some inferior images could be improved to the point where they could be evaluated. Still, some

images could not be improved sufficiently and had to be discarded.

For images that were acceptable, preprocessing algorithms reduced the effect of variations in staining intensity and the effects of colored masks and other anomalies. These preprocessing algorithms consisted of four distinct functions: verifying the image content, mask removal, contrast enhancement, and background removal (Supplementary Materials; Table S3 and “Details of image enhancement and ERA” section).

Epithelial recognition algorithms

Once the image was optimized through the various preprocessing algorithms,

the image was analyzed through ERAs which utilized both colorimetric (RGB) as well as intensity (grayscale) values (Supplementary Table S2). Epithelial cell detection initially utilized the Gaussian kernel. The ERAs initially created had to be further refined to more precisely define the area of identification (AOI) (Supplementary Materials; Tables S2, S4, S5, and S6 and “Details of image enhancement and ERA” section).

Calculating the epithelial area percentage

Once the epithelial area was defined in each FOV, the epithelial area percentage was calculated according to the following schema (Supplementary Table S7). The stromal area could be calculated as the reciprocal of the epithelial area. Epithelial percentage could vary from 0 to essentially 100%. The algorithm then ranked the FOVs by epithelial percentage and identified the highest 3–5 and earmarked these on the virtual slides for future TMA construction (Figure 2). Since some FOVs contained minimal tissue compared with the overall grid area, in those FOV the epithelial percentage could be artifactually elevated. To control for this possibility, FOVs whose total tissue area was <10% of the FOV area were automatically removed from further consideration (Supplementary Table S7).

Construction of TMAs

The TMAs were made from paraffin blocks containing human breast, colon and lung cancer tissues. We made three different types of TMAs and termed them manual TMA (manually selected cores, manually assembled into a TMA block), algorithmic TMA (algorithmically selected cores, manually assembled into a TMA block), and robotic TMA (algorithmically selected cores, robotically assembled into a TMA block). The manual TMA was constructed solely manually by the Ohio State University Research Pathology Core from the 300 retrieved cases. This manual selection required archival slide retrieval, re-review, manual circling of regions of interest, and alignment with the original tissue block from which the TMA was to be constructed. The TMA was made manually by selecting the three best areas, which were rich in cancer cells by matching the areas circled on the glass slide with corresponding regions of the paraffin block (Figure 3). Each core measured 1 mm in diameter and was spaced 0.8 mm apart on a single glass slide. Three 1-mm tissue cores from each formalin-fixed paraffin embedded donor block were selected

Table 2. Epithelial percentages (mean ± sd) of algorithmic TMA versus manual TMA

TMA	Algorithmic	Manual	P value
Breast	71 ± 10%	51 ± 7%	<i>P</i> < .01
Colon	68 ± 08%	45 ± 10%	<i>P</i> < .01
Lung	85 ± 12%	55 ± 14%	<i>P</i> < .001

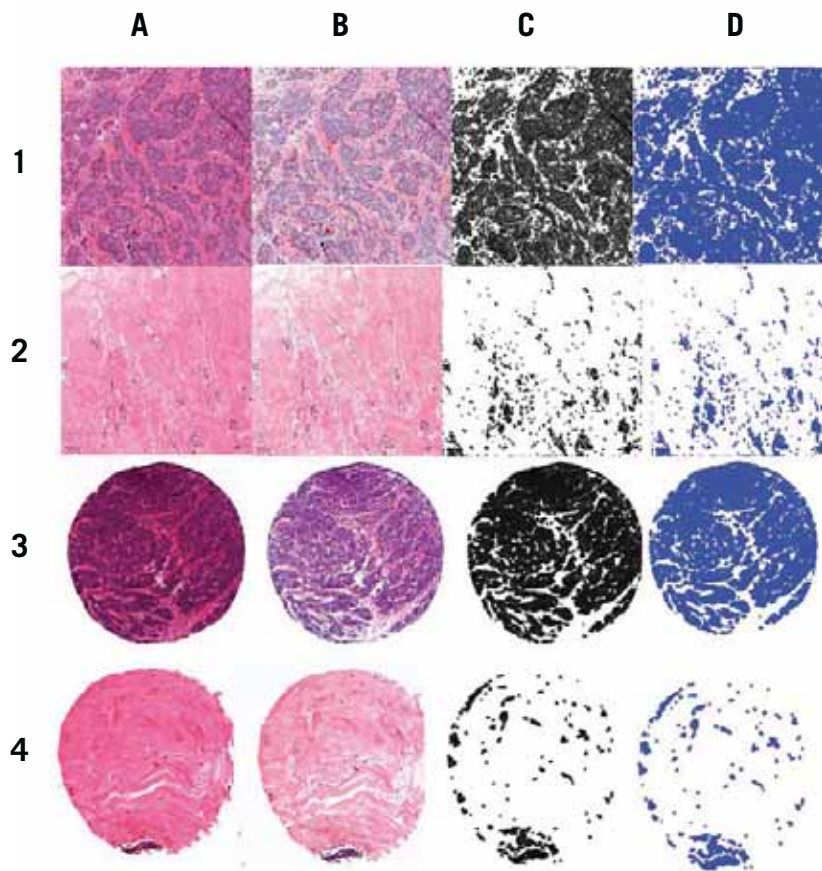


Figure 2. Processed images of algorithmically selected FOVs and algorithmic TMA cores versus manual TMA cores. Row 1, algorithmically selected FOV from whole slide with high epithelial percentage (85.11%); Row 2, algorithmically selected FOV from whole slide with low epithelial percentage (13.83%); Row 3, algorithmic TMA core with high epithelial percentage (cancer cell density) (85.4%); Row 4, manual TMA core with unacceptably low epithelial percentage (cancer cell density) (12.91%). Column A, H&E stained image; Column B, image processed by mask removal; Column C, contrast enhancement; Column D, epithelial area identification.

and precisely arrayed into a new recipient paraffin block. A previous study showed that ≥ 3 cores from each sample gave acceptable statistical analysis in TMAs in diverse tumor types (7); as such, the present work utilized similar multiple core sampling. The constructed TMAs were also subsequently scanned into virtual slides.

The algorithmic TMA was constructed from the same paraffin blocks under the guidance of the algorithms identifying those FOVs on the virtual slides with the highest cancer cell density. A trained technician used this grid as a template in making these algorithmically selected, manually assembled TMAs. TMA construction proceeded from this point in the same manner as manual TMA.

The robotic TMA was constructed using a robotic hardware device termed TMAker, which is operated under the control of the ERAs and FOV algorithms (Supplementary Materials; “Demonstration of TMAker” section). The device consists of a stacked carousel which can house up to 500 paraffin blocks and presents each block sequentially to two working stations: (i) a reading station where the identity of the block can be identified based on a barcode and the shape of the tissue contained within the block (by illumination) and compared with the corresponding virtual slide image contained in the database, and (ii) a coring station where an actuator arm, under the guidance of the algorithms, cores the areas of the block with the highest cancer cell density. The cores obtained are robotically deposited into a receiving block which eventually holds all of the cores of the TMA. This block is sectioned into slides, stained, and then scanned into virtual TMAs (Figure 3) in a manner identical to that used for both the manual TMA and the algorithmic TMA.

The same collection of paraffin blocks containing the 100 cases each of breast, lung, and colon cancer were used as the primary source material to derive the manual TMA, the algorithmic TMA, as well as the robotic TMA. Since these paraffin blocks contained fairly large tissue specimens, averaging ≥ 4 cm², there were at least 400 potential sites to core from each block so that both the manual TMA as well as the algorithmic TMA could easily be obtained from the same block. We first carried out the manual TMA and then the algorithmic TMA from the first paraffin block. We obtained the robotic TMA from the second paraffin block since the the algorithmic TMA had already directed the areas to be cored from the first block.

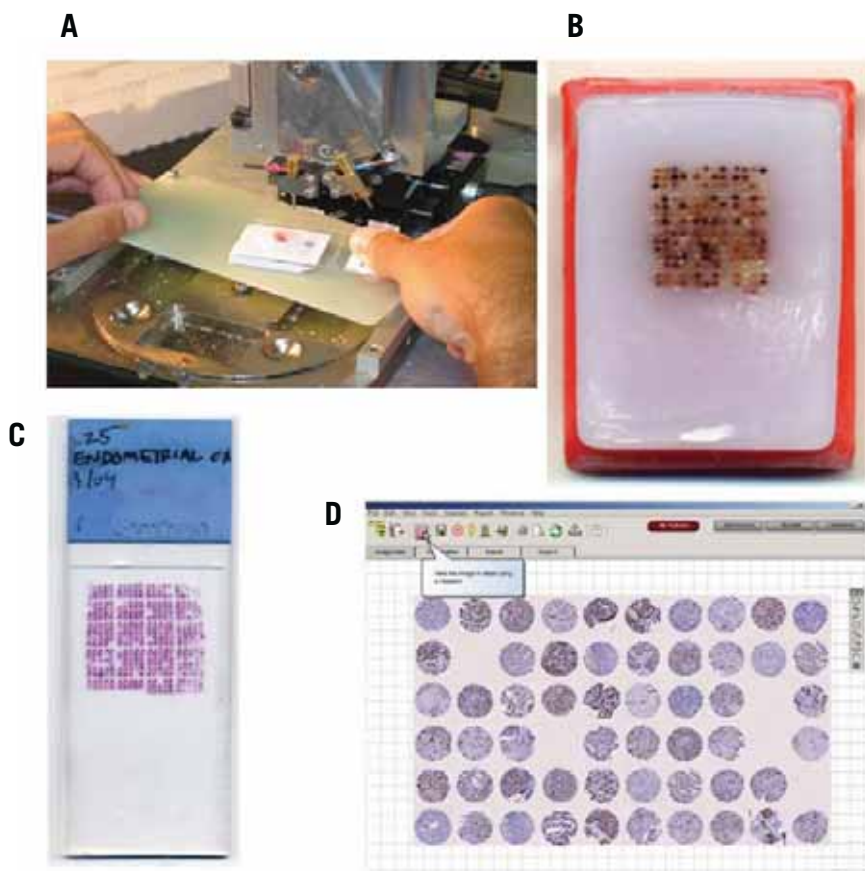


Figure 3. Comparison of manual versus robotic TMAs. Traditional manual TMA method of construction is depicted, where a glass slide containing circled areas of cancer cells, is overlaid over the corresponding paraffin block (A), producing a TMA block (B) and slide (C) with uneven rows and columns of cores. TMAker produces a robotic TMA that, in contrast to the manual TMA, has even rows and columns of cores (D). The robotic TMA-derived paraffin block is sectioned, scanned, and made into a virtual TMA.

Table 3. Epithelial percentages (mean \pm sd) of robotic TMA versus manual TMA

TMA	Robotic	Manual	P value
Breast	75 \pm 15%	53 \pm 8%	$P < .01$
Colon	72 \pm 10%	49 \pm 12%	$P < .001$
Lung	82 \pm 15%	58 \pm 12%	$P < .001$

Virtual slides of all three categories of TMA were independently assessed both algorithmically as well as manually by two raters (both pathologists) for epithelial cell (cancer cell) percentages. Estimates of epithelial cell (cancer cell) percentages of selected FOVs on the whole slides—as well as the TMA cores produced within all three categories—were also independently determined by these two raters and compared with the algorithmic measurements. The strength of these correlations was also determined.

Statistical methods

Intraclass correlations (ICCs) were calculated to assess the level of agreement among measurements of epithelial percentages. To calculate the ICC, intercept-only random

effects models were fit to the epithelial percentage with random effect variance components for tissue sample, rater, and error variance. The ICC was calculated as the variance component for tissue sample divided by the sum of the three variance components. Confidence intervals were calculated using the delta method.

For tests of the statistical significance of comparisons of epithelial cell percentages in different samples, Student's *t*-test was applied.

Software availability and accessibility

We have included a detailed code of the algorithms and a weblink to the algorithms.

Detailed code of the algorithms. Since the full source code of the algorithms is too

Table 4. Correlation of epithelial percentages among different depths of core sections in both algorithmic TMA and manual TMA

Tissue	Number of cases	Level	Intraclass correlation (95% confidence interval)
A) Algorithmic TMA			
Breast	100	I vs. II	0.84 (0.77, 0.91)
		II vs. III	0.93 (0.88, 0.98)
		I vs. III	0.82 (0.78, 0.86)
Colon	100	I vs. II	0.92 (0.88, 0.96)
		II vs. III	0.92 (0.85, 0.99)
		I vs. III	0.85 (0.75, 0.95)
Lung	100	I vs. II	0.86 (0.82, 0.90)
		II vs. III	0.86 (0.82, 0.90)
		I vs. III	0.84 (0.81, 0.87)
B) Manual TMA			
Breast	100	I vs. II	0.86 (0.75, 0.97)
		II vs. III	0.90 (0.86, 0.94)
		I vs. III	0.80 (0.78, 0.82)
Colon	100	I vs. II	0.88 (0.79, 0.97)
		II vs. III	0.89 (0.80, 0.98)
		I vs. III	0.86 (0.81, 0.91)
Lung	100	I vs. II	0.86 (0.82, 0.90)
		II vs. III	0.88 (0.81, 0.95)
		I vs. III	0.84 (0.77, 0.91)

Levels I, II, and III are relative depths through the blocks: I, superficial; II, midway; III, deep.

Table 5. Epithelial percentages (mean ± sd) of algorithmic TMA versus manual TMA averaged over depth of sectioning

TMA	Algorithmic	Manual	P value
Breast	82 ± 10%	58 ± 12%	<i>P</i> < .001
Colon	72 ± 10%	53 ± 14%	<i>P</i> < .01
Lung	86 ± 10%	62 ± 15%	<i>P</i> < .001

lengthy to provide in print, an abbreviated synoptic code that gives the essence of the source code is provided (Supplementary Materials; “Abbreviated synoptic code” section).

Weblink to the algorithms. A direct link to a demonstration of the ERAs—or a way to upload one’s own photomicrographs or scanned images for analysis with the ERAs—is the web site: <http://www.pathxchange.org>. Details to access this link are provided (Supplementary Materials; “Demonstration of web site link” section).

Results

Our specific FOV algorithms invariably could divide a whole virtual slide into a grid of FOVs. The number of FOVs that were needed to analyze the whole slide ranged 200–600 (average 400), depending on the size of the tissue specimen. The process of scanning each slide into a virtual slide took ~15 min and the process of gridding each slide into FOVs and analyzing each FOV algorithmically took an additional 15 min (Figure 1A; Supplementary Table S1).

Image acquisition by either the Aperio ScanScope T2 System or the iSCAN System produced equivalent results with

uniformly sharp images with high contrast. For approximately 10% of the images, mask removal and contrast enhancement improved image quality (Supplementary Table S3). The ERAs (Supplementary Tables S2, S4, S5, S6, and S7) applied to each FOV were successful in recognizing epithelium, filtering out stroma, and determining its epithelial percentage and therefore its cancer cell density.

For ~5% of the acquired images, the quality was below the standard necessary for the algorithms to interpret them. These images had to be discarded. Another 5% of the FOVs contained only a very small amount of tissue compared with the size of the given square (<10% tissue); these squares also had to be discarded because they falsely elevated the epithelial percentage (Supplementary Table S7).

After analyzing all the FOVs on a given slide, the algorithms ranked the FOVs on the basis of epithelial percentage and selected the 3–5 FOVs with the highest epithelial percentage (Figure 1B; Figure 2, row 1). FOVs with comparatively low epithelial percentage were identified but not selected (Figure 2, row 2). The algorithm-based determinations of

locations of those FOVs exhibiting the highest epithelial percentages were the same every time the algorithm was run and therefore showed no inter-observer, intra-observer, or fatigue variability.

There was a very strong agreement overall between all the algorithmic measurements of epithelial percentage made on the FOVs of a whole virtual slide and the subjective measurements of the same made by the two raters (Table 1).

In order to compare the manual, algorithmic, and robotic TMAs, we began with algorithmic measurements of epithelial percentage made on the FOVs of a whole virtual slide. The slide coordinates of the three FOVs with the highest epithelial percentage (as determined by the algorithms) were used to guide both manual construction of the TMA (algorithmic TMA) as well as construction by TMAker (robotic TMA) (Supplementary Material; “Demonstration of TMAker” section). The cores produced in both the algorithmic TMA and robotic TMA reflected high cancer cell density. Algorithmic TMA cores are depicted (Figure 2, row 3). In contrast, manual TMA based on subjective slide template alignment and manual construction often produced cores with comparatively low epithelial percentages and low cancer cell densities (Figure 2, row 4). These cores would be considered less informative.

The results of our comparative study of manual, algorithmic, and robotic TMA showed that algorithmic TMA contained cores with epithelial cell (cancer cell) percentages which were ~50% higher overall in cancer cell density than those of manual TMA. This observation held true for breast (*P* < 0.01), colon (*P* < 0.01), and lung (*P* < 0.001) TMAs (Table 2). What makes this comparison even more impressive is that the manual TMA had the first sampling of the tissue block, yet the algorithmic TMA produced cores of a higher epithelial (cancer cell) density. Robotic TMA showed a similar increase in overall cancer cell density compared with manual TMA (Figure 3, A–C). These observations held true across different TMAs: breast (*P* < .01), colon (*P* < .001), and lung (*P* < .001) (Table 3). The robotic TMA had an essentially equivalent epithelial (cancer cell) density to the algorithmic TMA (data not shown), but produced a TMA of even rows and columns of cores (Figure 3D).

We then compared the depth of sections of the TMA cores created by manual, algorithmic, and robotic TMA. At various levels—superficial, midway, and deep (nearly full thickness)—into the TMA block, there was a

strong agreement among the epithelial percentages of all three depths for both manual and algorithmic TMA (Table 4, A and B). However, the increase in overall epithelial cell (cancer cell) percentages in the algorithmic TMA versus manual TMA held when compared at the various depths (Table 5). Results for the robotic TMA were similar to the results for the algorithmic TMA (data not shown). In all of these studies, the measurements of epithelial cell (cancer cell) percentages on both the whole slide FOVs as well as the final TMA virtual cores were algorithmically determined. However, there was also a very strong agreement overall between algorithmic epithelial cell (cancer cell) percentage measurements made on the virtual TMAs and the subjective measurements of the same made by the two raters (data not shown) just as there had been with the whole slide FOV comparisons (Table 1).

Our ERAs were not perfect and there were some examples of both false negative and false positive epithelial recognition. Infiltrating lobular carcinomas of the breast, because they consist of small epithelial cells, sometimes could not be detected adequately and gave rise to false negative epithelial recognition. Some lymphoid aggregates, because they consisted of cellular clumps, were often considered by the algorithm to be epithelial in nature and gave rise to false positive epithelial recognition. A weblink demonstration of the ERAs showing both true positivity and true negativity, as well as false negativity and false positivity, is provided (<http://www.pathxchange.org>). Details to access this link are provided (Supplementary Materials; “Demonstration of web site link” section).

It should be emphasized, however, that in the vast majority of FOVs, the ERAs recognize true positivity from true negativity. It should be remembered that the purpose of the ERAs and FOVs is to divide a slide into grids and select the areas with the highest epithelial percentage to

guide TMA construction. Even if some grids show some degree of false negativity or false positivity, this would not change the overall effectiveness of the ERAs in guiding TMA construction because most of the FOVs would be interpreted accurately by the ERAs.

Discussion

The main benefits of both algorithmic and robotic TMA in guiding TMA construction are increased efficiency and the removal of human error. Since manual TMA reflects the current standard, the advantages of both algorithmic TMA and robotic TMA should be determined based on a comparison with this standard.

Manual TMA presently involves retrospective manual selection of cases which require archival slide retrieval, re-review, manual circling of regions of interest, and alignment with the original tissue block from which the TMA is constructed. This process is quite time consuming, taking weeks to months.

We wish to point out that the main issue herein was not to test whether the algorithmic TMA or robotic TMA is superior to manual TMA in producing a higher density of epithelial cells. Our focus was whether TMA construction could be automated and whether a robot could replace a human being. Indeed, even if both automated TMA and robotic TMA yielded equivalent results to manual TMA in terms of epithelial cell density, the automated approach would still be highly advantageous.

Using this algorithm-driven technology, glass slides of potential cases which are candidates for future TMA construction can be prospectively scanned and made into a library of virtual slides. These virtual slides can then be analyzed with our ERAs and FOV algorithms and the regions mapped for TMA production. Slide scanning and algorithmic analysis each take approximately 15 min per slide, but if it is done at the time of routine

pathological slide review, it can create a library of virtual slide images and identify prospective cancer regions during the course of pathologists’ everyday work load. This information then can be used to guide construction of either algorithmic TMA, or robotic TMA with TMAker. Overall, scanning and algorithmic analysis leading to either algorithmic TMA or robotic TMA is presently much faster and efficient than for manual TMA, reducing the overall time from weeks or months to hours (11–13).

The present study demonstrated that both algorithmic TMA and robotic TMA are superior to manual TMA in identifying areas of the slide with a higher epithelial percentage and, therefore, a higher cancer cell density. This observation held across different cancer types (breast, colon, and lung). However, the overall significance of this observation is unclear. Although it cannot be presumed that more is necessarily always better, the presence of a greater epithelial percentage may improve signal detection, and that this is where the automated technology platform particularly excels compared with manual methods.

Furthermore, if one remembers that automated TMA construction is only the first step in ultimate TMA analysis where ERAs and subsequent specific-recognition algorithms (SRAs) will be applied to analyze immunoreactivity in tumor cells but not stroma, certainly cores richer in tumor cells will be more easily analyzed and either false negatives or false positives from stromal contamination will be minimized. This is the reason that the increase in cancer cell density by the automated approach is desired. However, in order to generally show that molecular data obtained on epithelial cell-enriched tissue arrays are more representative or clinically relevant than manual arrays, we first must produce and then analyze these arrays algorithmically.

Although we have not demonstrated that increased epithelial percentage adds value from the standpoint of added clinical information, from another perspective increased epithelial percentage does add value. In general, grids with the very highest epithelial percentages are likely to contain invasive cancer because normal epithelium—especially in the breast, colon, and lung—exhibits a much lower epithelial percentage. These higher epithelial percentages are the very reason why the algorithmic approach is desired. Our imaging algorithms will not directly distinguish carcinoma in situ from invasive carcinoma; however, increased epithelial



**CALIBRATION
SERVICES LLC**

Committed to Quality Pipette Service

At MEU Calibration Services quality and precision is the cornerstone of our work and customer satisfaction is our commitment. We repair and calibrate all brands of pipettes including, but not limited to Rainin, Eppendorf, Gilson and Brand.

Visit us at meucalibrationservices.com or call us at 609-556-8660

percentages can indirectly help distinguish these areas. Those grids with the highest epithelial percentages are more likely to contain invasive carcinoma than carcinoma in situ because usually carcinoma in situ is surrounded by a higher percentage of non-epithelial stroma.

TMA's are made and interpreted manually by a time-consuming process (14–16). In contrast, analogous cDNA microarrays and genomic libraries are made and interpreted rapidly, because both construction and interpretation are computer-driven (17,18). cDNA microarray technology is highly automated and high-throughput with relatively manageable biological material. The largest cDNA arrays now spot over 2 million features per slide, and it is possible that DNA microarrays may eventually be replaced with high-throughput sequencing in the near future. TMA's, on the other hand, have not yet advanced to this stage. Unless fully automated in both construction as well as interpretation (as in robotic TMA), TMA technology will never approach the high-throughput profiling capabilities of cDNA microarrays.

Manual TMA's have traditionally been limited to 1–3 cores per sample (7), although the optimal number of cores to reduce limited sample bias is still controversial. The optimal number of cores and the optimal epithelial percentage directly address an optimal data representation issue. This issue notwithstanding, one of the benefits of the robotic TMA approach is that the technology platform presented is flexible in allowing a variable number of cores, depending on the heterogeneity of the marker being studied. As more and more tumor biomarkers and tumor-associated signaling pathways are investigated, the varying degree of heterogeneity within tumors for various antigens and signaling pathways may require a range in the number of cores per patient sample to overcome limited sample bias. For example, Her-2/neu immunoreactivity in breast cancer is usually fairly homogeneous and one core may be sufficient; on the other hand, estrogen receptor (ER) immunoreactivity in breast cancer is more heterogeneous and three cores may be necessary. In studying selected phosphorylated transcription factors like p-ETS, even more heterogeneity may be present, requiring a significantly greater number than three cores per case. Certainly any robotic TMA construction system that can produce as many cores as desired from a given sample—for so-called “multiplex” TMA's—would be poised to determine what value overcomes limited sample bias

for any given antigen. There are no real tissue limitations of multiplex TMA's. Multiplex TMA manufacturing will not completely consume the tumor. Most tumors removed from patients are made into multiple whole slides with corresponding paraffin blocks, and there are usually several blocks available. The typical slide obtained from the block contains an area of tumor that is 2 cm × 2 cm (4 cm², or 400 mm²). A typical TMA core is 1 mm in diameter. Therefore, ~400 or more cores can be derived from one paraffin block. Even if 10 cores are produced from each block, this consumes only 2.5% of the tumor. If the algorithm ranks the areas of cancer cell density, it would be fairly easy to select the 10 areas with the highest density without compromising or exhausting the block.

In conclusion, the use of ERAs and FOV algorithms on virtual slides to guide TMA selection and ultimately TMA construction will result in TMA's becoming truly part of biomarker high throughput screening.

Acknowledgments

This study was supported by The Donald A. Senhauser Endowment of the Ohio State University (awarded to S.H.B.)

Competing interests

S.H.B. serves as Chief Medical Officer of BioImagene, Inc. (uncompensated) but is a minority stock holder. K.B. serves as a compensated consultant to BioImagene, Inc. A.S.G. and A.S.B. are employees of BioImagene, Inc. L.G. and R.E.J. declare no competing interests.

References

- Natkunam, Y., R. Warnke, K. Montgomery, B. Falini, and M. van de Rijn. 2001. Analysis of MUM1-IFR4 protein expression using tissue microarrays and immunohistochemistry. *Mod. Pathol.* 14:686–694.
- Torhorst, J., C. Bucher, J. Kononen, P. Haas, M. Zuber, O.R. Kochli, F. Mross, H. Dietrich, et al. 2001. Tissue microarrays for rapid linking of molecular changes to clinical endpoints. *Am. J. Pathol.* 159:2249–2256.
- Barsky, S.H. 2003. Myoepithelial mRNA expression profiling reveals a common tumor-suppressor phenotype. *Exp. Mol. Pathol.* 74:113–122.
- Liu, C.L., W. Prapong, Y. Natkunam, A. Alizadeh, K. Montgomery, C.B. Gilks, and M.V.D. Rijn. 2002. Software tools for high-throughput analysis and archiving of immunohistochemistry staining data obtained with tissue microarrays. *Am. J. Pathol.* 161:1557–1565.
- Kononen, J., L. Bubendorf, A. Kallioniemi, M. Barlund, P. Schrami, S. Leighton, J. Torhorst,

- M.J. Mihatsch, et al. 1998. Tissue microarray for high-throughput molecular profiling of tumor specimens. *Nat. Med.* 4:844–847.
- Ross, J.C. 1994. *The Image Processing Handbook*; 2nd ed. CRC Press, Boca Raton, FL.
- Rubin, M.A., R. Dunn, M. Strawderman, and K.J. Pienta. 2002. Tissue microarray sampling strategy for prostate cancer biomarker analysis. *Am. J. Surg. Pathol.* 26:312–319.
- Gonzalez, R.C. and R.E. Woods. 1992. *Digital Image Processing*. Addison-Wesley, Upper Saddle River, NJ.
- Jain, A.K. 1989. *Fundamentals of Digital Image Processing*, Prentice-Hall, Inc., Upper Saddle River, NJ.
- Pal, S.K. and A. Ghosh. 1992. Image segmentation using fuzzy correlation. *Inf. Sci.* 62:223–250.
- Sharangpani, G.M., A.S. Joshi, K. Porter, A.S. Deshpande, S. Keyhani, G.A. Naik, A.S. Gholap, and S.H. Barsky. 2007. Semi-automated imaging system to quantitate estrogen and progesterone receptor immunoreactivity in human breast cancer. *J. Microsc.* 226:244–255.
- Joshi, A.S., G.M. Sharangpani, K. Porter, S. Keyhani, C. Morrison, A.S. Basu, G.A. Gholap, A.S. Gholap, and S.H. Barsky. 2007. Semi-automated imaging system to quantitate Her-2/neu membrane receptor immunoreactivity in human breast cancer. *Cytometry A* 71:273–285.
- Haedicke, W., H.H. Popper, C.R. Buck, and K. Zatlouka. 2003. Automated evaluation and normalization of immunohistochemistry on tissue microarrays with a DNA microarray scanner. *BioTechniques* 35:164–168.
- Mobasheri, A., R. Airley, C.S. Foster, G. Schulze-Tanzil, and M. Shakibaei. 2004. Post-genomic applications of tissue microarrays: basic research, prognostic oncology, clinical genomics and drug discovery. *Histol. Histopathol.* 19:325–335.
- Simon, R., M. Mirlacher, and G. Sauter. 2004. Tissue microarrays. *BioTechniques* 36:98–105.
- Manley, S., N.R. Mucci, A.M. Marzo, and M.A. Rubin. 2001. Relational database structure to manage high-density tissue microarray data and images for pathology studies focusing on clinical outcome: the prostate specialized program of research excellence model. *Am. J. Pathol.* 159:837–843.
- Ginestier, C., N. Cervera, P. Finetti, S. Esteyries, B. Esterni, J. Adelaide, L. Xerri, P. Viens, et al. 2006. Prognosis and gene expression profiling of 20q13-amplified breast cancers. *Clin. Cancer Res.* 12:4533–4544.
- Barlund, M., O. Monni, J.D. Weaver, P. Kauraniemi, G. Sauter, M. Heiskanen, O.P. Kallioniemi, and A. Kallioniemi. 2002. Cloning of BCAS3 (17q23) and BCAS4 (20q13) genes that undergo amplification, overexpression, and fusion in breast cancer. *Genes Chromosomes Cancer* 35:311–317.

Received 19 October 2006; accepted 15 September 2009.

Address correspondence to Sanford H. Barsky, M.D., Department of Pathology, University of Nevada School of Medicine, 1 Manville Medical Building, University of Nevada, Reno, NV, 89557. email: sbarsky@medicine.nevada.edu